Meteoritics & Planetary Science 44, Nr 4, 603–620 (2009)
Abstract available online at http://meteoritics.org

Predictions for the LCROSS mission

D. G. KORYCANSKY[1*], Catherine S. PLESKO[1, 2], Martin JUTZI[3], Erik ASPHAUG[1], and Anthony COLAPRETE[4]

[1]CODEP, Department of Earth Sciences, University of California, Santa Cruz, California 95064, USA
[2]Los Alamos National Laboratory, Los Alamos, New Mexico 87545, USA
[3]Physikalisches Institut, Sidlerstrasse 5, 3012 Bern, Switzerland
[4]245-3 NASA Ames Research Center, Moffett Field, California 94035, USA
[*]Corresponding author. E-mail: kory@pmc.ucsc.edu

(Received 14 July 2008; revision accepted 07 January 2009)

Abstract–We describe the results of a variety of model calculations for predictions of observable results of the LCROSS mission to be launched in 2009. Several models covering different aspects of the event are described along with their results. Our aim is to bracket the range of expected results and produce a useful guide for mission planning. In this paper, we focus on several different questions, which are modeled by different methods. The questions include the size of impact crater, the mass, velocity, and visibility of impact ejecta, and the mass and temperature of the initial vapor plume. The mass and velocity profiles of the ejecta are of primary interest, as the ejecta will be the main target of the S-S/C observations. In particular, we focus on such quantities as the amount of mass that reaches various heights. A height of 2 km above the target is of special interest, as we expect that the EDUS impact will take place on the floor of a moderate-sized crater ~30 km in diameter, with a rim height of 1–2 km. The impact ejecta must rise above the crater rim at the target site in order to scatter sunlight and become visible to the detectors aboard the S-S/C. We start with a brief discussion of crater scaling relationships as applied to the impact of the EDUS second stage and resulting estimated crater diameter and ejecta mass. Next we describe results from the RAGE hydrocode as applied to modeling the short time scale ($t \leq 0.1$ s) thermal plume that is expected to occur immediately after the impact. We present results from several large-scale smooth-particle hydrodynamics (SPH) calculations, along with results from a ZEUS-MP hydrocode model of the crater formation and ejecta mass-velocity distribution. We finish with two semi-analytic models, the first being a Monte Carlo model of the distribution of expected ejecta, based on scaling models using a plausible range of crater and ejecta parameters, and the second being a simple model of observational predictions for the shepherding spacecraft (S-S/C) that will follow the impact for several minutes until its own impact into the lunar surface.

For the initial thermal plume, we predict an initial expansion velocity of ~7 km s^{-1}, and a maximum temperature of ~1200 K. Scaling relations for crater formation and the SPH calculation predict a crater with a diameter of ~15 m, a total ejecta mass of ~10^6 kg, with ~10^4 kg reaching an altitude of 2 km above the target. Both the SPH and ZEUS-MP calculations predict a maximum ejecta velocity of ~1 km s^{-1}. The semi-analytic Monte Carlo calculations produce more conservative estimates (by a factor of ~5) for ejecta at 2 km, but with a large dispersion in possible results.

INTRODUCTION

In 2009, NASA will launch the Lunar Reconnaissance Orbiter (LRO) mission to the Moon. Riding along will be the Lunar Crater Observation and Sensing Satellite mission (LCROSS). LCROSS consists of a 2000 kg impactor and a shepherding spacecraft (S-S/C). After separation and release of LRO, the spent second stage of the rocket (EDUS) will be directed on a course that will impact the Moon. The likely target at present writing will be the floor of a permanently shadowed crater at one of the lunar poles. The S-S/C will follow closely behind the impactor to observe impact and subsequent ejecta before impacting the lunar surface itself some 4 minutes later. The impact velocity will be approximately that of lunar escape (2.5 km s^{-1}) and the impact angle from the horizontal will be in the range of ~60–80°.

The primary goal of LCROSS is the search for and characterization of subsurface water that may be present in the lunar soil. Aside from the considerable scientific interest of the question, the possible presence of near-surface water is a resource for human exploration and colonization of the Moon. The instruments aboard the S-S/C will search for and characterize the presence or absence of water at the impact site at the 0.5% level.

In this paper, we present results of modeling the second-stage impact using a variety of approaches and computer models. After a discussion of modeling considerations, we apply empirical crater scaling relationships to estimate the expected size and mass of the crater and the ejecta. We follow this with a report of the outcomes of various modeling calculations. We start first with a model of the generation of the initial thermal plume (over a time scale $t \sim 0.07$ s) using the RAGE code, followed by two independent calculations of the ejecta using two codes employing different techniques (smooth particle dynamics, or SPH, and finite differences, using the ZEUS-MP code). We then present a semi-analytic Monte Carlo calculation of the ranges of expected outcomes of the impact, based on scaling relations. We end with discussion of the expected observations by the S-S/C based on a simple model of scattered sunlight from the ejecta curtain. Shuvalov and Trubetskaya (2008) have also produced numerical models of the LCROSS impact using the SOVA code. We will compare our results to their predictions.

Modeling Considerations

The ideal procedure would be to generate predictions of impact effects that are unique and tightly constrained. Such predictions would have the maximum benefit for analysis of the LCROSS experiment and yield the maximum amount of information about the characteristics of the target site. However, our modeling capabilities are not yet up to the challenge of modeling the impact in full detail. Uncertainties about the target are significant. In particular, we lack (and will continue to lack) knowledge about the regolith, especially its strength and porosity, and the thickness of any loose soil layer above bedrock. The properties of the lunar surface at the sub-kilometer scale vary significantly over the entire surface. The surface regolith varies from 2–20 m in depth, and grades from a surface of fine silt with bulk density 1660 kg m^{-3} and 40% porosity through larger scale ejecta, blocky fractured crust, down to competent bedrock roughly 25 km below the surface. The geochemical composition of the lunar crust varies somewhat, although much less than that of Earth. It is largely space-weathered basalt, basalt glass, and anorthosite (Heiken et al. 1991).

In addition, modeling the impact event is computationally very challenging. The impacting rocket stage is a thin-walled aluminum cylinder with additional internal structure. The rocket stage wall thickness is ~0.01 m, far too small to resolve in a hydrodynamical computation that must also span many meters of the target. Even the most advanced codes have difficulties in realistically representing the material characteristics of the lunar surface and its response to a relatively low-speed (~2.5 km s^{-1}) impact. To our knowledge, computer modeling of a hollow cylinder hitting porous regolith has not been achieved by any modeling group in a validated manner. At this stage, with the resources available to us, we can produce only partial models of various stages and processes that we expect to occur during and after the impact.

The different calculations we present here made different assumptions for the impactor structure. In the discussion of the predictions from crater scaling relations, the effects of different assumptions about the gross characteristics of the impactor (dimension, average density) could be included in a very basic way. The RAGE calculations modeled the impactor as a cube of aluminum at full density (2700 kg m^{-3}), while for the ZEUS-MP calculation the impactor was taken to be a low-density “cloud” (30 kg m^{-3}) of material of the same dimension and mass as the EDUS. A more realistic structure was used for the SPH calculations: two full plates separated by 10 m, in addition to a homogeneous impactor model similar to that used for the ZEUS-MP calculations. Two calculations were done in which the orientation of the plates differed (horizontal versus vertically) with respect to the vertical impact velocity vector. The SPH calculations address to some degree the question of how much the results depend on assumptions about impactor structure. As seen in Fig. 7 (discussed below), the amount of ejecta mass at high velocities (and thus reaching greater heights, 10 km about the surface or more) may be the quantities that are most sensitive to details of the EDUS structure.

Surface roughness of the target is also a factor contributing to modeling challenges, as discussed below; whether the target is a loose regolith (and how deep it is) or composed of boulders (and how large they might be). In various models we make some attempts at addressing this factor.

Goals of this Paper

Our aim is to bracket the range of expected results and produce a hopefully useful and robust guide that has helped and will continue to help with mission planning. The various tools at our disposal include analytic results derived from decades of experiments reported in the literature as summarized in the form of scaling relations, as well as hydrodynamic simulations. We have aimed the various calculations at the differing aspect of the problem for which each method was suited; no one method is capable of following the entire process from end to end. To some extent this shapes our inquiries and the structure of this paper reflects this fact.

The mass and velocity profiles of the ejecta are of primary interest, as the ejecta will be the main target of the S-S/C observations. In particular, we will focus on such quantities as the amount of mass that reaches various heights. A height of 2 km above the target is of special interest, as we expect that the EDUS impact will take place on the floor of a moderate-sized crater of ~30 km in diameter, with a rim height of 1–2 km. The impact ejecta must rise above the crater rim at the target site in order to scatter sunlight and become visible to the detectors aboard the S-S/C.

In this paper, we focus on several different questions, which are modeled by different methods. The questions include the following, for which we also the code and/or method(s) that we used to attack the problem.

- How large will the impact crater be? (Crater scaling, ZEUS-MP, SPH)
- How much ejecta will be generated by the impact, and how fast will it move? (Crater scaling, ZEUS-MP, SPH, Monte Carlo calculations)
- How hot will the initial impact vapor plume be? (RAGE)
- How visible will the impact ejecta be? (Semi-analytic model of the ejecta observations)

CRATER SCALING

Empirical formulae have long been available to estimate the size of impact craters as a function of projectile characteristics such as mass, velocity and angle. In general, the formulae derive from analysis of non-dimensional combinations of impactor and crater properties, that have been found to be related by power laws (Holsapple and Schmidt 1982; Housen et al. 1983; Holsapple 1987, 1993). Parameters (coefficients and power-law indices) are found from analysis of experiments and are generally assumed to hold in regimes that may be far removed from those to which we have experimental access. In some cases, clever experimental set-ups allow the substitution of an experimental regime to planetary one without extrapolation (as with experiments in high-gravity centrifuges, (Schmidt and Holsapple 1980)). Additionally, numerical calculations provide support for extrapolation of scaling relations (O'Keefe and Ahrens 1993).

Theoretical analysis usually proceeds on the assumption of a "point-source" approximation, in which the impactor dimension is assumed to be small compared to the resulting crater and any structural characteristics (such as a hollow structure) are ignored. A few experiments have investigated impactors that are non-point-like (Schultz and Gault 1985), a situation that is especially relevant to LCROSS as the dimensions of the EDUS (10 × 3 m) will be comparable to the resulting crater. We address this issue only indirectly in this section, by means of the density scaling below. In the SPH calculations (section ZEUS-MP Results), we show results of a pair of simulations in which the impactor structure is modeled more directly.

In general, two regimes of cratering are distinguished, the "strength regime," for small events into intact targets, in which the target material strength determines the final crater size, and the "gravity regime" in which the event is large enough, or the target is weak, so that gravitational stresses are much larger than the material strength. For the LCROSS impact, as noted, the site characteristics will be unknown until the impact. Should the EDUS strike a rocky surface, the crater will be formed in the strength regime. On the other hand, if the target is loose regolith, the gravity regime will probably be more appropriate, leading to a crater as much as twice as large as in the strength regime, with several times the volume of ejecta. For the remainder of this discussion we will posit a gravity-regime impact into a regolith target.

Gravity-regime crater volumes V can be related to impactor characteristics by a relation among non-dimensional groups π_V, π_2, and the density ratio (ρ/δ):

$$\pi_v = K\pi_2^{-\frac{3\mu}{2+\mu}}\left(\frac{\rho}{\delta}\right)^{\frac{6v-2-\mu}{3\mu}}, \quad \text{where } \pi_v = \frac{\rho V}{m}, \pi_2 = \frac{ga}{U^2} \qquad (1)$$

(Holsapple 1993), where δ is the impactor density, m the impactor mass, a is the impactor radius, g is the gravity, and U is the vertical component $U = V \sin\theta$ of velocity of an impactor striking the surface at total velocity V and angle θ from the horizontal (for vertical impacts, $\theta = 90°$). The coefficient K and power-law indices μ and ν are determined from experiments. Additionally, if the impactor density δ differs from the target density ρ, there is a dependence on the ratio of the two as noted. For strength-regime craters, a similar relation holds, involving the group $\pi_3 = Y/\rho U^2$, where Y is the material strength. A convenient website for calculating predicted crater diameters D, depths d, and ejecta masses m_e has been set up by Holsapple (2007)[1], based primarily on relations given by Holsapple (1993). For gravity-regime craters in lunar regolith, the parameters are taken to be $K = 0.132$, $\mu = 0.41$, $\nu = 0.33$, and target density $\rho = 1700$ kg m^{-3}.

One question that comes up is the effect of impactor density. As noted above, the EDUS is a hollow structure consisting of a thin-walled aluminum cylinder with a rocket motor at one end. The average density of a 2000 kg structure of dimensions 10 × 3 m is $\rho = 28$ kg m^{-3} with an equivalent spherical diameter of 5.14 m. Alternatively, one can assume that the impactor can be modeled by a solid sphere of the same mass, for which applying the density of aluminum gives an impactor diameter of 1.12 m. Assuming a vertical impact at $U = 2.5$ km s^{-1}, both cases can be entered into the web-form at Holsapple's site, yielding the D, the "apparent" diameter of the crater that is below the original surface (the $z = 0$ plane), rim-to-rim diameter D_R, and ejecta masses m_e of 13.7 m, 17.8 m, and 2.91×10^5 kg for the low-density case and corresponding

[1] http://keith.aa.washington.edu/craterdata/scaling/index.htm

values of $D = 17.5$ m, $D_R = 22.8$ m, and $m_e = 6.05 \times 10^5$ kg for the full-density impactor case.

From numerical simulations, O'Keefe and Ahrens (1993) find the relation $D/a = 2.1\pi_2^{-0.22}$, where the exponent corresponds to a value $\mu = 0.56$. Plugging in the full-density impactor numbers yields a diameter $D = 37.5$ m, more than twice as large as the Holsapple values given above, but smaller than the value for a water impact (for which the Holsapple's website gives $D = 59.0$ m and $m_e = 4.07 \times 10^7$ kg).

Members of the LCROSS science team (private communication) have independently produced a range of estimates and a consensus "Common Best Estimate Impact Model" (CBEIM) for the crater and ejecta characteristics. The CBEIM parameters are $D = 16.9$ m, $D_R = 20$ m, and $m_e = 4.95 \times 10^5$ kg. Science team estimates for the ranges of crater diameter and ejecta mass are $13 < D < 22$ m, $17 < D_R < 23$ m, and $2.5 \times 10^5 < m_e < 1.0 \times 10^6$ kg.

RAGE MODELING OF THE THERMAL PLUME

We used the RAGE hydrocode to model the initial thermal plume of hot impactor and target material that is expected to develop on short time scales (~0.1 s) after the impact.

RAGE is a version of the SAIC Adaptive Grid Eulerian hydrocode (Gittings et al. 2008). It is a compressible Eulerian hydrodynamics code that uses continuous Adaptive Mesh Refinement (AMR) to follow discontinuities with a fine grid while treating the bulk of the simulation more coarsely. RAGE simulations may be carried out in one, two, or three dimensions, and in Cartesian, cylindrical, or spherical coordinate systems. It was originally designed to model strong shocks in ocean water, which required that the code be able to model the effects of water depth, a wide variety of material types, and to calculate shock and flow field details to second order accuracy over large time and distance ranges. To do this, the code uses a direct-Eulerian Godunov finite difference treatment of the conservation equations. The direct-Eulerian Godunov model breaks the calculation down into an initial Lagrangian step followed by an Eulerian step. In the Lagrangian step, the Riemann problem is solved for each volume element according to the method described by Hartenet al. (1983). The results of the Lagrangian step are remapped to Eulerian coordinates, where the Eulerian versions of the Navier-Stokes equations are used to calculate updated values of the conserved quantities. RAGE is second order accurate in time and space in uniform regions (Kamm and Rider 1998), and first-order at discontinuities, which is a fundamental property of Godunov schemes.

A variety of equations of state are available to RAGE. Of these, the most accurate is SESAME. SESAME is a temperature-based tabular equation of state maintained by the Mechanics of Materials and Equations of State group at Los Alamos National Laboratory. The table for each material has an associated unique and thermodynamically consistent fit of semi-empirical theoretical models appropriate to different temperature or pressure regions to experimental data. (Johnson 1994) The majority of SESAME equations of state follow a Mie-Gruneisen model at lower energies and Thomas-Fermi-Dirac theory at higher energies. Debye theory is used to handle solids, and empirical data are used for phase transitions. In addition to the SESAME equations of state, RAGE uses a Steinberg-Guinan strength model, which tracks the stress, and models strength in terms of the stress resulting from resistance to shearing. Our model is of a simple solid block of aluminum striking a strength-less but solid basalt surface at 2.5 km s^{-1}. It ran on 128 EV68 1.25 GHz processors in the LANL QSC unclassified supercomputing cluster.

Approximations and Scaling

The parameters used in the RAGE simulation are simplified from the actual problem in order to make the calculation possible.

Challenges Posed by Complicated Targets and Impactors

This impact is a challenging case to model for a variety of reasons. The target surface is not well characterized. The impactor itself is a complicated object made of a variety of materials including metals, composites, and volatiles, in thin layers with large voids throughout. A detailed model of the exact impact would require three dimensional CAD representations of the impactor and surface, sub-centimeter resolution over a volume of at least 1 km^3, and more processing power than is currently available. The size and energy of the impact are such that the impact processes are neither purely strength dominated (smaller, lower energy) nor purely gravity dominated (larger, higher energy). This regime of impact cratering is a topic of current research, but not sufficiently well characterized for detailed and exact predictions.

Physical Model Simplifications

The simplest, fastest model to run is that of a solid aluminum block of a mass similar to that of the kinetic impactor. The target regolith is modeled as a homogeneous, strengthless basalt. This allows the target to respond more like a powder without requiring a complicated treatment of large porosity values.

Geometric Simplifications

The Courant condition for numerical models requires that the model's timestep, Δt, must be small enough that a wave does not propagate more than one grid cell-length, Δx during Δt. Using the above physical model simplification for the impactor, we would require $\Delta x < 0.5$ m for the proper mass distribution. This leads to extremely tiny timesteps, which makes the calculation unwieldy and introduces adverse

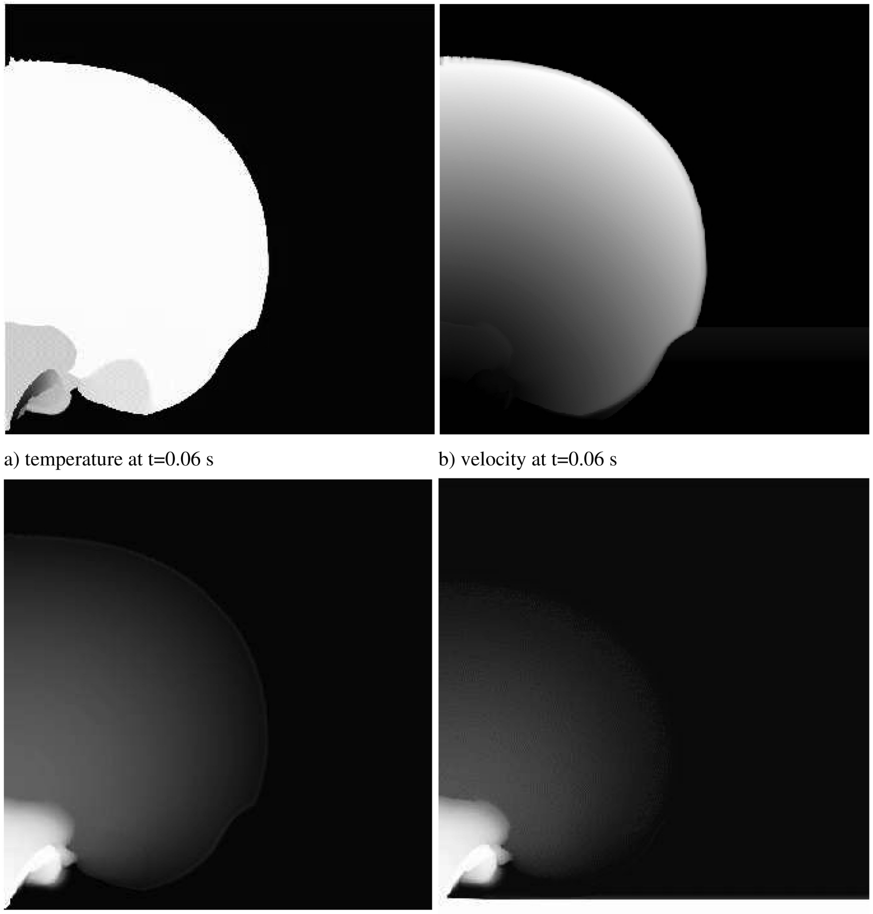

a) temperature at t=0.06 s b) velocity at t=0.06 s

c) aluminum density at t=0.06 d) basalt density at t=0.06

Fig. 1. RAGE calculation. a) Temperature contours of the initial plume at $t = 0.06$ s. The color scale is linear from 0 K (black) to 1230 K (white). b) Velocity contours of the initial plume at $t = 0.06$ s. The gray scale is linear from 1 km s^{-1} (black) to 7 km s^{-1} (white). c) Contours of aluminum density in the initial plume at $t = 0.06$ s. The gray scale is logarithmic from 10^{-33} kg m^{-3} (black) to 1000 kg m^{-3} (white). d) Contours of basalt density in the initial plume at $t = 0.06$ s. The gray scale is logarithmic from 10^{-33} kg m^{-3} (black) to 1000 kg m^{-3} (white).

numerical effects. To make the computation tractable, we have rescaled the problem. In section 7.4 of his cratering book, Melosh (1989) outlines hydrodynamic similarity arguments that allow an impact problem to be "scaled up" by multiplying length scales by a constant factor. Schmidt and Holsapple used these scaling arguments in their centrifuge cratering experiments. In this work, we used a scaling factor of 10, enough to increase the timestep to a computationally feasible value.

Effects of Simplifications

The densities of the target and impactor are assumed to be completely homogeneous at the standard density of the materials of which they are made. The following estimates are upper limits on the amount and velocity of ejecta thrown out by such a cratering event. In a more realistic event, time and energy will be taken up by crushing the spacecraft and the regolith during the impact. This means that in these simplified models there is more energy available to heat and eject material from a smaller projectile-target interface, compared to realistic scenarios where energy is taken up by compaction and spread out over a larger projectile-target interface, leaving more energy in the simplified models available to vaporize target material at the point of impact. How much of an effect this would have is at present difficult to quantify.

Vapor Results

The plume was modeled out to a 0.5 km radius from the impact point, over a period of 0.07 s. It has a maximum temperature of 1230 K, above the low-pressure vaporization points for both basalt (1034 K, 0.089 eV) and aluminum (1160 K, 0.1 eV) predicted by the SESAME equation of state, and contains both materials from the earliest stages of the plume.

Figure 1 shows results of the RAGE calculations at t = 0.06 s. Included in the figure are plots of the temperature, density of aluminum and basalt, and the velocity field of the plume. Figure 2 shows the height, diameter, and mass of the plume as a function of time in the top panel. The plume expands roughly hemispherically, with a maximum radial

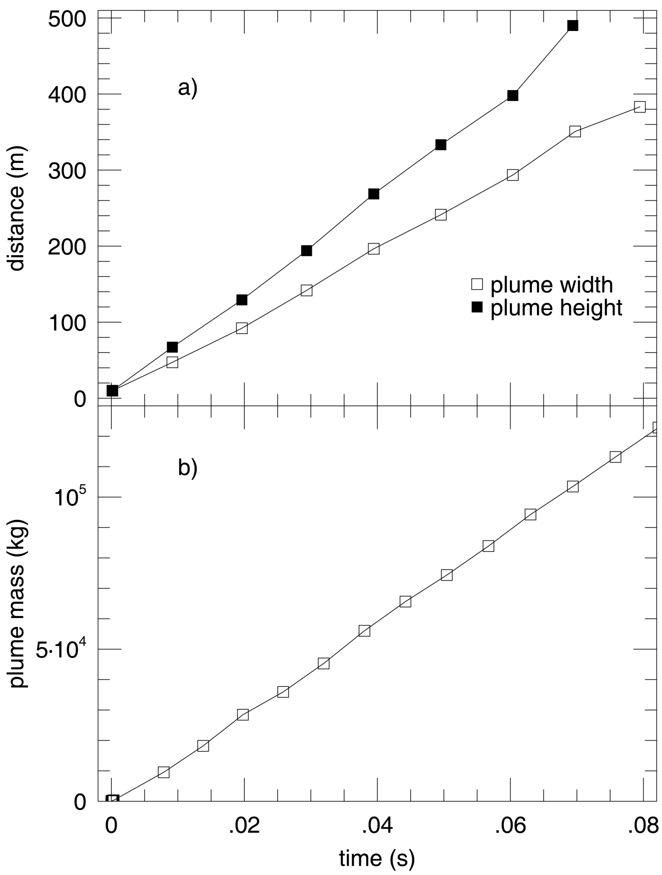

Fig. 2. RAGE calculation: Top panel: Plot of vapor plume height and diameter versus time. Bottom panel: Plot of vapor plume mass versus time.

velocity of 7 km s^{-1}. By $t = 0.07$ s it has expanded to a height of ≈0.5 km. The bottom panel of Fig. 2 shows the plume mass as a function of time in the same calculation. The amount of mass increases linearly with time. By $t = 0.07$ s the amount of ejecta mass in the plume is ≈10^5 kg.

Given that the plume expands to be much larger than the impactor (even scaled up as described), we expect that these results (plume dimensions, temperature, and velocity) will be largely independent of the scaling. Plume mass (and density) however, is expected to scale with the impactor mass.

SPH RESULTS

We now turn to larger-scale modeling of crater formation and ejecta. The first models we describe are Smooth Particle Hydrodynamics (SPH) results. We have used an SPH impact code to study the initial phase of the crater formation. In particular, we investigated the ejecta velocity distribution and the provenance (initial position in the target) of the ejecta for different target and projectile types.

The standard gas dynamics SPH approach was extended by Benz and Asphaug (1994) to include an elastic-perfectly plastic material description (see, e.g., Libersky and Petschek [1991]) and a model of brittle failure based on the one of Grady and Kipp (1980). Therefore, our SPH impact code can be used to model impacts and collisions involving solid bodies in the strength- and gravity-dominated regime. This method has been successfully tested on different scales Benz and Asphaug (1994); Michel et al. (2001). Recently, our SPH impact code was extended to include a porosity model. The model is based on the so called "$P - \alpha$" model (Herrmann 1969) which was adapted for implementation in the code (Jutzi et al. 2008).

Using our 3D SPH impact code, we performed several simulations of the LCROSS impact, considering different properties of the target. Three different target types were investigated:

1. A flat surface, target density: 1800 kg m^{-3} (target T1).
2. A flat surface, target density: 1800 kg m^{-3}, porosity (33%) is explicitly modeled (target T2).
3. A small hill (6 m) on an otherwise flat surface, target density: 1800 kg m^{-3} (target T3).

The target is modeled as a pre-damaged (i.e., strengthless) basalt, and the Tillotson equation of state (EOS) is used. Since the bulk density of the lunar regolith is expected to be lower than the one of basalt (ρ_0 = 2700 kg^{-3}), we used ρ_0 = 1800 kg m^{-3} for targets T1 and T3. However, for target T2 ρ_0 = 2700 kg m^{-3} is used, resulting again in an initial density of 1800 kg m^{-3} (due to the porosity of 33%).

For all simulations presented here, we used ~3.5 million SPH particles placed in a half sphere of 30 m radius. This results in a particle mass of ~25 kg and a spatial resolution of ~0.25 m. The impactor is modeled as an underdense (ρ = 30 kg m^{-3}), 3 × 10 m aluminum cylinder with a mass of 2020 kg. The impact velocity is 2.5 km s^{-1} and the impact angle 70°.

Figure 3 shows the outcome of the three simulations after 0.6 s in two dimensional slices of the three dimensional target. The colors label the z-component of the velocity, positive values indicating ejection. For the same simulations, the maximum height of the ejecta is shown in Fig. 4, where the fraction of material ejected from different target layers is also plotted. Interestingly, the provenance of most of the ejecta is near the surface ($z_0 > -1$ m) in all three cases (see also Fig. 5). Due to the small hill the third calculation (target T3), there is almost no material ejected from depths below $z_0 = -1$ m. As can be seen, there is generally less ejecta in the target T2 (where porosity is explicitly modeled), than in target T1 (where we do not model porosity but only adjust the initial density). Table 1 indicates the total mass ejected above a certain height for the three simulations.

In order to investigate the dependence of the results on the projectile characteristics (geometry, density), we also performed simulations using different projectile types, to

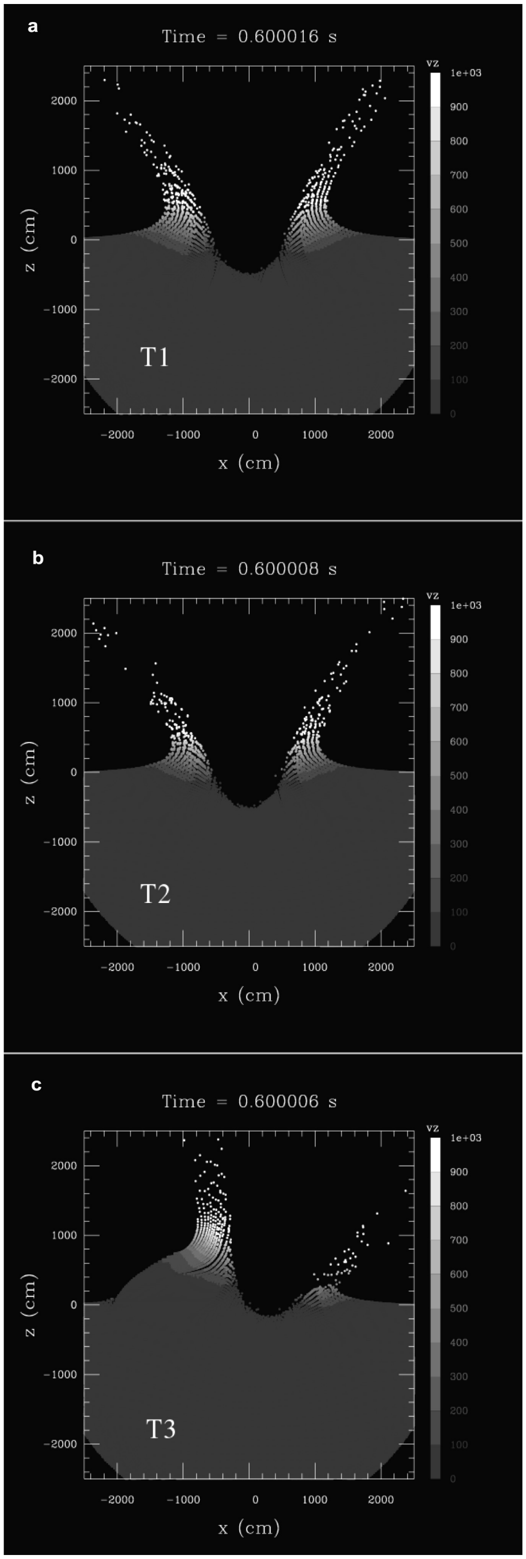

Fig. 3. SPH calculations: two dimensional slices of three dimensional targets showing the locations and vertical velocity (in cm s^{-1} on a linear scale) of the SPH particles at $t = 0.6$ s. Results are shown for targets T1 (flat surface, density $\rho = 1800$ kg m^{-3}) (top left), T2 (flat surface, density $\rho = 1800$ kg m^{-3}, 33% porosity) (top right), and T3 (6 m hill, density $\rho = 1800$ kg m^{-3}) (bottom).

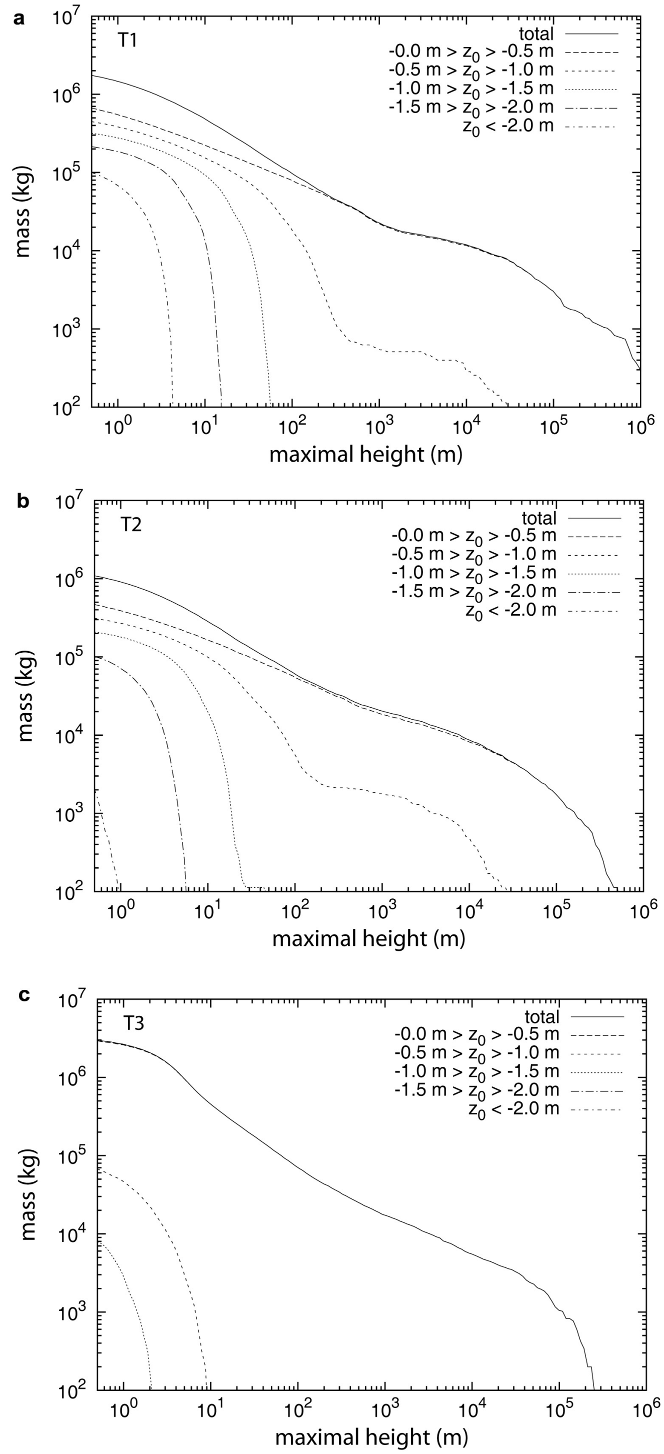

Fig. 4. SPH calculations: mass of material $m(>z)$ that reaches height z or greater as a function of height z. Results are shown for targets T1 (flat surface, density $\rho = 1800$ kg m^{-3}) (top left), T2 (flat surface, density $\rho = 1800$ kg m^{-3}, 33% porosity) (top right), and T3 (6 m hill, density $\rho = 1800$ kg m^{-3}) (bottom). The various dotted and dashed lines give the provenance (depth below the surface z_0) of the ejecta material for the indicated values of z_0.

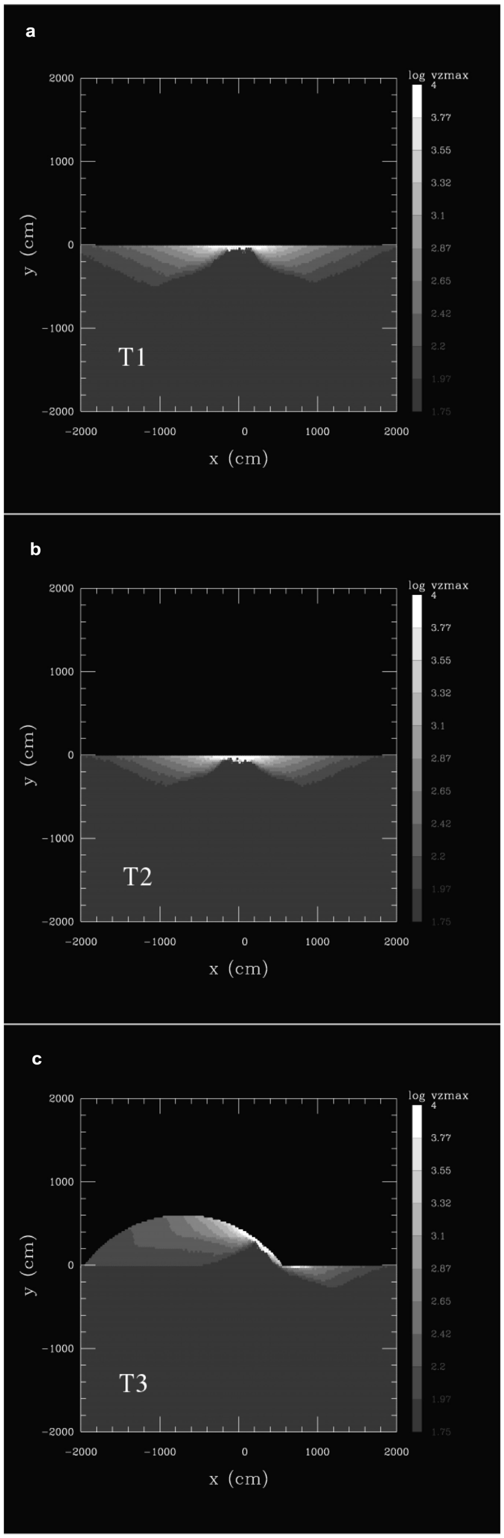

Fig. 5. SPH calculations: maximum vertical velocity reached by the SPH particles as functions of the initial position in the targets. Velocities are shown on a logarithmic scale. Results are shown for targets T1 (flat surface, density $\rho = 1800$ kg m^{-3}) (top left), T2 (flat surface, density $\rho = 1800$ kg m^{-3}, 33% porosity) (top right), and T3 (6 m hill, density $\rho = 1800$ kg m^{-3}) (bottom).

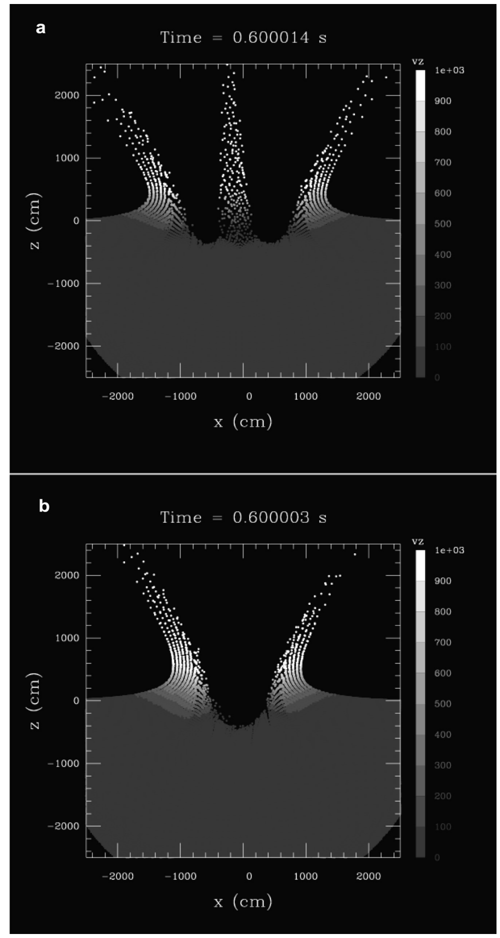

Fig. 6. SPH calculation: two dimensional slices of the three dimensional target showing the positions and vertical velocity (cm s^{-1}) of SPH particles at $t = 0.6$ s. In these simulations, the impactor consists of two parallel plates 3 m in diameter, 10 m apart. The plates are oriented so that the axis connecting them lies parallel to the target surface (left image) or perpendicular to the target surface (right image).

Table 1. Amount of mass (kg) ejected above height z (SPH calculations).

z (km)	m (kg, T1)	m (kg, T2)	m (kg,T3)
0.1	9.5×10^4	5.9×10^4	6.9×10^4
1	2.2×10^4	2.0×10^4	1.7×10^4
10	1.2×10^4	8.6×10^3	1.5×10^3
100	2.6×10^3	1.5×10^3	1.0×10^3

Table shows the amount of mass reaching various heights in the SPH calculations. Columns are height z, and the amount of mass m in kg reaching height z in kg, for impacts into targets T1, T2, and T3.

examine the effects (if any) of the EDUS geometry and mass distribution. For these simulations, we used a projectile which consisted of two parallel plates 3 m in diameter that were 10 m apart. Each of the plates had a mass of 510 kg and a density of 2700 kg m^{-3}. The axis of the "projectile" is oriented along the impact direction or rotated by 90 degrees

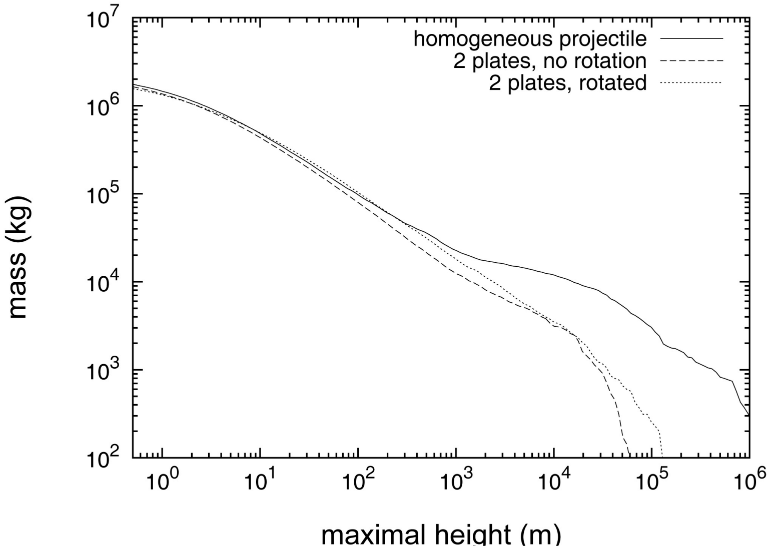

Fig. 7. SPH calculation: Mass of $m(>z)$ material that reaches height z or greater as a function of height z. Results are shown for the parallel plate calculations shown in Fig. 6. The target type is T1.

(which means that the plates impact at different target positions). We used target T1 for these simulations. Figures 6 and 7 show the outcome of the two simulations after 0.6 s. In Fig. 7, the maximum height of the ejecta obtained by these simulations is compared to the simulation with the homogeneous projectile. As can be seen, there is more material ejected above 10 km using the homogeneous projectile, which means that more high speed ejecta is produced in this case. On the other hand, the velocity distribution at lower velocities (corresponding to heights <10 km) looks very similar in all three cases. Interestingly, the orientation of the projectile does not seem to strongly influence the velocity distribution of the ejecta. However, different orientations of the projectile can obviously lead to different crater morphologies.

ZEUS-MP RESULTS

We have also made calculations of the initial phase of crater formation using the three-dimensional hydrodynamics code ZEUS-MP (Norman 2000), which we have modified for multi-material calculations of atmospheric impacts (Korycansky et al. 2002, 2006; Korycansky and Zahnle 2003). ZEUS-MP is an Eulerian solver of the equations of compressible hydrodynamics. Our calculations were done in Cartesian geometry. The size of the domain is 400 × 400 × 500 m ($-100 < z < 400$ m). The calculation shown here follows the events of the first 4 s after impact. The grid size is 128 × 128 × 158, with horizontal resolution of 3.12 m, and a non-uniform vertical grid with a minimum resolution of 1.72 m at the surface. The grid expands geometrically with a factor of 1.01 per cell for $z < 0$ and $0 < z < 60$ m and 1.04 for $z > 60$ m.

The EDUS is modeled as a 10 × 3-m cylinder of density = 30 kg m^{-3}, impacting at $v = 2.5$ km s^{-1}. The target density is 2700 kg m^{-3}. Above the surface is a low-density background medium with density 10^{-6} kg m^{-3} and pressure 0.1 Pa. The crater attains its maximum depth at $t = 2.3$ s. ZEUS-MP does not contain a material strength model, so the calculations are pure "gravity regime" calculations, and the equation of state is a very simple one known as the Murnaghan EOS (Melosh 1989).

Figure 8 shows slices through the three-dimensional density field of a ZEUS-MP calculation of the EDUS impact with parameters described above. Examination of the results (Fig. 9) shows that the ZEUS-MP calculation produces a crater that is several times larger and deeper than predicted from scaling relations such as those of Holsapple (2007). Although the dimensions predicted for water impacts are approximately the same as those from ZEUS-MP regolith calculations in this case. The crater dimensions calculated from the scaling relations O'Keefe and Ahrens (1993) are somewhat closer, though approximately a factor of two smaller. The reason for this result from ZEUS-MP is not understood at present.

The large crater produced from the ZEUS-MP calculation results in a large amount of impact ejecta as shown in Fig. 8 at various stages of the calculation. Maximum velocities of up to 1 km s^{-1} are produced in the calculation. A plot of the ejecta mass velocity distribution from the calculation is shown in Fig. 10. Overall, the mass-vs-velocity distribution is satisfactory. The total ejecta mass is 10–100 times larger than predicted from crater and ejecta scaling relation. There is a range from ~10–500 m s^{-1} over which there is an apparent power-law distribution. The cutoff at larger velocities (~1 km s^{-1}) and its time dependence (i.e., the

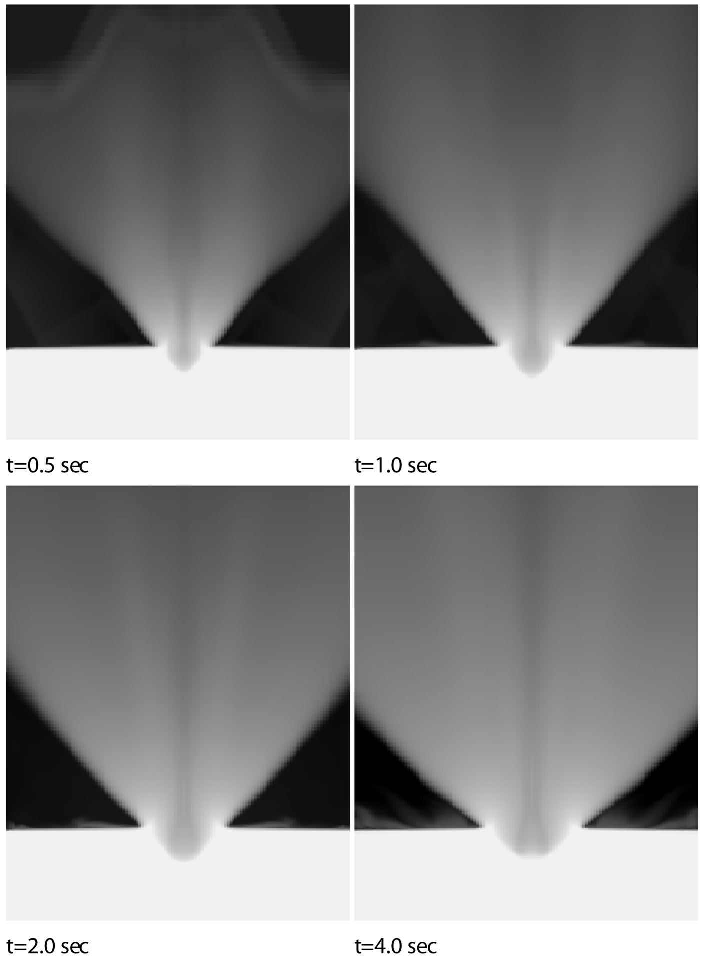

Fig. 8. ZEUS-MP calculation: density slice through mid-plane of three dimensional calculation of the impact of a low-density cylinder representing the EDUS. The dimensions of the plots are $-0.2 < x < 0.2$ km by $-0.1 < z < 0.429$ km. Density slices are shown at $t = 0.5$, $t = 1.0$, $t = 2.0$, and $t = 4.0$ s. The density scale is logarithmic $10^{-6} < \rho < 10^4$ kg m^{-3}.

drop in the distribution for the later times) is consistent with material flowing out the boundaries of the grid as the calculation progresses.

Comparing the SPH and ZEUS-MP calculations, we find, as noted, that ZEUS-MP simulation produces a much bigger crater (and far more ejecta) than are made in the SPH calculations. For the SPH target T1 calculation, the crater diameter at $t = 0.6$ s is $D = 11.7$ m, and the depth $d = 5.4$ m. The SPH crater is both smaller and deeper than that predicted by the usual crater scaling rules, but it is likely that at the end of the SPH calculation, the crater has not yet completed its formation. The ZEUS-MP calculation at $t = 0.6$ has corresponding values of $D = 35$ m and $d = 22$ m, about 40 times greater volume. The velocity distribution of the ejecta is similar, however, when the difference in total mass is taken into account. We regard the ZEUS-MP results as less reliable than the others, however. We believe that the crater size and ejecta mass from the EDUS impact calculations are more likely to reflect the results of the SPH calculations, crater scaling relations, and the calculations by Shuvalov and Trubetskaya (2008).

Shuvalov and Trubetskaya (2008) simulated the impact of spheres and hollow spherical shells of aluminum and iron into porous rocky surface (with strength effects) using the SOVA code. They followed the calculation up to $t = 0.2$ s, and found a crater diameter of $D \sim 11$ m and $d \sim 3$ m at that point. The velocity distribution of the ejecta was quite similar to the SPH results: $\sim 2 \times 10^5$ kg, with a maximum velocity of ~ 1 km s^{-1}. The ZEUS-MP calculations (as seen in Fig. 10) produced a maximum velocity of ~ 0.7 km s^{-1} at $t = 0.5$ s. All three sets of calculations show a small amount of material (10^2–10^3 kg) lifted to altitudes of a few hundred km. Given the uncertainties in the calculations and assumptions about the impactor and target, we regard the predictions about high altitude material ($z > 100$ km) as highly uncertain.

MONTE CARLO MODELS OF THE EJECTA

This model is based on the ejecta-scaling rules given by Housen et al. (1983). Ejecta are shot outward and upward at a constant angle $\theta \approx 45°$ from the horizontal, and the ejecta velocity v at radial position x, and volume $V_e(<x)$ of ejecta x,

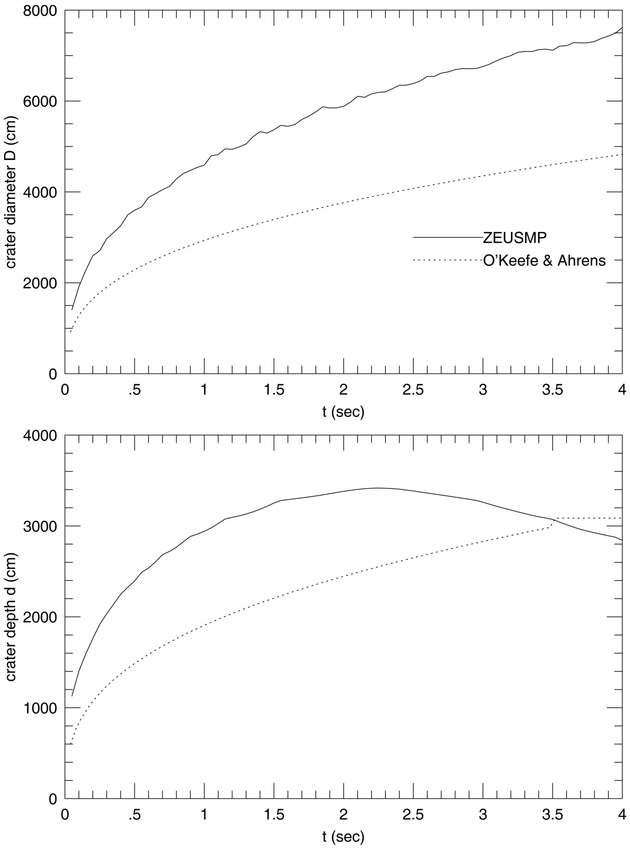

Fig. 9. ZEUS-MP calculation: crater diameter (top) and depth (bottom) as a function of time for the calculations shown in Fig. 8 (solid lines). For comparison, diameter and depth from O'Keefe and Ahrens (1993) are also shown (dashed lines).

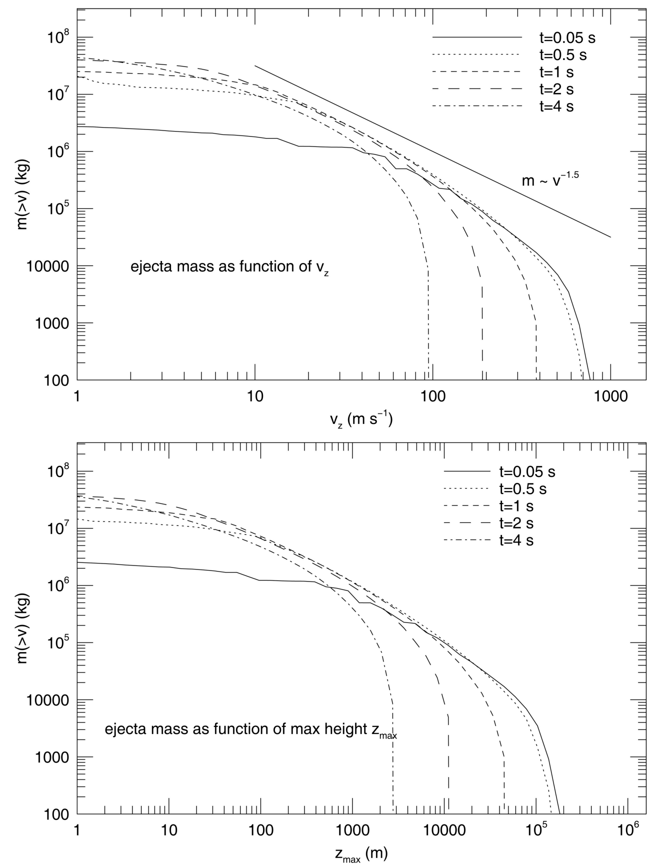

Fig. 10. ZEUS-MP calculation: mass-velocity relation for ejecta from the impact simulation shown in Fig. 3. The amount of mass $m(>v)$ moving at velocity v or greater is shown at times $t = 0.05$, $t = 0.5$, $t = 1$, $t = 2$, and $t = 4$ s. For comparison, the power law $m \propto v^{-1.5}$ is also indicated. The target is a full-density surface ($\rho = 2700$ kg m^{-3}). Top: ejecta mass $m(>v)$ as a function of v_z. Bottom: ejecta mass $m(>v)$ as a function of maximum height z_{max}.

in a crater of radius R are given by

$$\frac{v}{\sqrt{gR}} \propto \left(\frac{x}{R}\right)^{(\alpha-3)/2\alpha}, \quad \frac{V_e(<x)}{R^3} \propto \left(\frac{x}{R}\right)^3. \qquad (2)$$

As before, we assume that all ejecta are launched instantaneously from the origin at $t = 0$. The cumulative distribution of the amount of ejecta mass m launched with velocity V or greater as

$$m(>V) = M_e \frac{\left[\left(\frac{V}{v_{min}}\right)^{6\alpha/(\alpha-3)} - \left(\frac{v_{max}}{v_{min}}\right)^{6\alpha/(\alpha-3)}\right]}{\left[1 - \left(\frac{v_{max}}{v_{min}}\right)^{6\alpha/(\alpha-3)}\right]}, \qquad (3)$$

where M_e is the total mass of ejecta. Ejecta are assumed to move ballistically in a vertical gravitational field with lunar gravity $g = GM_{moon}/R^2_{moon} = 1.63$ m s^{-2}. (For the relevant time and length scales, the results are virtually the same as those obtained with a $1/R$ potential, as discussed below.) An ejectum follows the path $X(t)$, $Z(t)$:

$$X(t) = V\cos\theta t, \quad Z(t) = V\sin\theta t - \frac{1}{2}gt^2. \qquad (4)$$

We calculated the amount of ejecta mass M($>v$) moving faster than specified velocities and the maximum amount of mass $M_{max}(z)$ that reaches (or exceeds) a set of specified heights z. For the latter quantity, the amount of mass at or above height z is a function of time and is a maximum at $t_{max} = (2z/g)^{1/2}$. The corresponding launch velocity is $V_0 = (z + gt^2_{\max}/2)/t_{max} \sin\theta$. For the particular model above, calculating these quantities is very simple, given t_{max} and V_0. Note the t_{max} is a function of z and g only and so has the same values no matter what the other parameters are. We give the values of t_{max} for each height z in Table 2.

Another set of results is the predicted radius of the ejecta curtain. In our model, the inner radius of the curtain can be found from Equation 3, by setting $Z = 0$ and solving for X by eliminating V. For a given value of t (e.g., t_{max}), the curtain radius $X_0(t) = (gt^2\cot\theta)/2$. For $t = t_{max}$, $X_0 = z\cot\theta$. The outer radius of the curtain is not well defined: the surface density of the ejecta curtain is a monotonically decreasing function of X (or Z) and the apparent outer edge will depend the sensitivity of the detector and other parameters such as particle size and detector integration time.

Table 2. Non-Monte Carlo model results using CBEIM: fraction of ejecta mass moving at velocity v or greater.

v ms^{-1}	% mass fraction
10	23.5
50	2.10
100	0.74
250	0.18
450	0.072
800	0.0265
1800	0.0033

Table shows the mass fraction moving at velocity v or faster, using the ejecta scaling law of Housen et al. (1983) and the common best-estimate model parameters (CBEIM) for the impact crater. Columns are velocity v, and the mass fraction moving at velocity v or faster.

Table 3. Non-Monte Carlo model results using CBEIM: amount of mass above height z.

z (km)	kg	t_{max} (s)
2	3.00×10^3	50
5	1.49×10^3	79
10	8.73×10^2	111
15	6.36×10^2	136
25	4.23×10^2	175
35	3.22×10^2	207

Table shows the amount of mass reaching various heights using the scaling law of Housen et al. (1983) and the common best-estimate model parameters (CBEIM) for the impact crater. Columns are height z, and the amount of mass m in kg reaching height z, and the time at which the maximum amount of material is a heights $\geq z$.

The Monte Carlo aspect of the model consists of choosing N sets of random values of the model parameters (with a specified distribution in a given range) and evaluating the resulting distribution $M(>v)$ and $M_{max}(z)$. The results depend on the distribution of the model parameters, and so they should be interpreted with that in mind.

The basic parameters in the model are $v_{min} = (gR_{crat})^{1/2}$, α and M_e, θ, and the maximum ejecta velocity v_{max}. We used the range of estimates provided by the LCROSS science team to set the limits in the models: $6.5 < R_{crat} < 11$ m, and $2.5 \times 10^5 < M_e < 1 \times 10^6$ kg. In principle M_e is a function of R_{crat}. However, given the uncertainties in crater geometry and regolith density and depth, we thought it better to treat M_e as an independent model parameter. (A slightly more consistent treatment would be to use the volume associated with a given value R_{crat} as an upper limit on ejecta volume.) For α we used the range between momentum and energy scaling ($3/7 < \alpha < 3/4$), and for θ the range $0.2\pi < \theta < 0.3\pi$. For the first set of models to be discussed, we set $v_{max} = v_{esc} = 2.38$ km s^{-1}; model results with different (lower) values of v_{max} are discussed below.

For comparison, we first calculated model predictions for a single set of parameter values, namely the "best estimate" numbers: $R_{crat} = 8.95$ m and $M_e = 4.95 \times 10^5$ kg. For α and θ we choose $\alpha = 3/5$ and $\theta = 45°$. Model results for this set of parameters are shown in Tables 2 and 3.

It is useful to examine the values that result from allowing one parameter at a time to vary. To save space, the results are not tabulated here, but examination of them shows that the results are most sensitive to the value of α that is chosen for the model. This follows naturally from the power-law dependence of the ejecta mass on velocity. Unfortunately, α is probably the least well constrained parameter in the model.

Tables 4 and 5 show the results for the Monte Carlo simulations (for $N = 50{,}000$ trials) as described above. In this case we tabulate the values for the minimum, maximum, median and mean results. Also, we include the values for the lower 10th and upper 90th percentiles, to give some feel for the distributions of the results, which are quite non-gaussian. The median results are not very different from the single-value best-estimate numbers shown in Table 2, but the distribution of possible results is very wide, especially for the maximum mass has a function of height. Figures 11 and 12 shows the distribution of results; note that the x-axes of the panels are logarithmic.

One of the uncertainties is the maximum velocity of the ejecta. Tables 2–5 were generated using models in which the maximum ejecta velocity v_{max} equaled the escape velocity ~2.4 km s^{-1}, as noted above. However, it is possible that v_{max} will be significantly smaller, as by the ZEUS-MP results and Shuvalov and Trubetskaya (2008), for which v_{max} ~1 km s^{-1}. The question is under current investigation experimentally as well (P. Schultz, private communication). We have thus run sets set of Monte Carlo calculations in which 0.2 km s^{-1} $< v_{max} < v_{esc}$. Figures 13 and 14 show the quantities given in Tables 4 and 5 as a function of v_{max}. Long-dashed lines show the minimum model (lower line) and maximum model (upper line). Short-dashed lines show $m(>v_z)$ values for the 10% (lower line) and 90% models. The dashed line shows that average value and the dotted line the median value of $m(>v_z)$ for the given value of v_z As might be expected, the amounts of material predicted at high velocities and reaching correspondingly high altitudes is most sensitive to v_{max}. The amount of material reaching low altitudes (e.g., 2 km, just clearing the expected crater rim height) is not very sensitive to this parameter.

Comparison between the Monte Carlo calculations and the SPH calculation show that the Monte Carlo calculations are in general more conservative in their predictions of the amount of mass reaching various heights. The SPH calculations predict that 2.6 $\times 10^4$ kg will reach our fiducial altitude of 2 km, for the case in which the EDUS is modeled as a homogeneous object. The two cases in which the EDUS is modeled as two flat plates are more conservative, approximately 10^4 kg will reach 2 km. For the Monte Carlo calculations, the median prediction is ~4 $\times 10^3$ kg, with only ~10% of the cases predicting masses above 10^4 kg. For the Monte Carlo cases in which $v_{max} = 300$ m s^{-1}, masses at 2 km are reduced by a factor of ~2. More precise predictions can be found by a comparison of Table 1 (for the SPH calculations)

Table 4. Monte Carlo models: Fraction (%) of ejecta mass moving at velocity v or greater.

v (ms^{-1})	Min.	10%	Med.	Avg.	90%	Max.
10	10.6	15.2	23.6	24.3	34.5	41.8
50	0.43	0.74	2.21	2.78	5.85	8.21
100	0.11	0.20	0.79	1.14	2.71	4.02
250	0.017	0.035	0.20	0.35	0.94	1.50
450	0.0051	0.011	0.080	0.16	0.46	0.76
800	0.0015	0.0034	0.030	0.068	0.20	0.35
1800	0.00014	0.00035	0.0038	0.010	0.31	0.56

Table shows the mass fraction moving at velocity v or faster, using Monte Carlo models based on the ejecta scaling law of Housen et al. (1983). Columns are velocity v and values of the fraction of ejecta mass characterizing the distribution of results: the minimum, 10% value, median, average, 90% value, and maximum value, produced by the suite of models.

Table 5. Monte Carlo models: Ejecta mass (kg) at or above altitude z.

z (km)	Min.	10%	Med.	Avg.	90%	Max.
2	1.65×10^2	8.55×10^2	3.76×10^3	6.00×10^3	1.48×10^4	3.75×10^4
5	6.63×10^1	3.62×10^2	1.90×10^3	3.34×10^3	8.63×10^3	2.32×10^4
10	3.31×10^1	1.88×10^2	1.12×10^3	2.13×10^3	5.69×10^3	1.59×10^4
15	2.19×10^1	1.27×10^2	8.22×10^2	1.63×10^3	4.43×10^3	1.27×10^4
25	1.30×10^1	7.79×10^1	5.50×10^2	1.16×10^3	3.20×10^3	9.41×10^3
35	9.16×10^0	5.59×10^1	4.19×10^2	9.17×10^2	2.57×10^3	7.69×10^3

Table shows the amount of mass reaching various heights, using Monte Carlo models based on the ejecta scaling law of Housen et al. (1983). Columns are height z and amount of mass m (in kg) reaching height z characterizing the distribution of results: the minimum, 10% value, median, average, 90% value, and maximum value, produced by the suite of models.

and V. The results of Shuvalov and Trubetskaya (2008) are similar, yielding ~10^4 kg at 2 km.

SIMPLE MODEL OF THE OBSERVATIONS

We present a simple model of some expected observations to be made by the S-S/C after the EDUS impact. We calculate the height and radius of several contours of mass per unit area dm/dA of the ejecta curtain and their apparent diameter as seen from the S-S/C. We base the model on ejecta curtain dynamics as described by Housen et al. (1983).

In this case, we modeled the lunar gravity field as the full $1/R$ lunar potential (though for $t < 1000$ s, there is not much difference in the results from assuming a constant vertical gravity field). The initial condition is that particles are launched from $X = Y = 0$, $Z = R_{moon}$ in a coordinate system with an origin at the Moon's center and initial velocity $V_x = V \cos\theta$, $V_z = V \sin\theta$. Given the launch position and velocities, one can calculate the positions X, Y, and Z of the ejecta at time t as a standard problem in a Keplerian potential (Bond and Allman 1996). The loci of the ejecta at time t mark out an approximately conical surface of area A. We calculate the surface density (mass per unit area of the ejecta curtain) dm/dA along the ejecta curtain as a function of height (or radius) and time from the impact point, using V as a parameter. Finding the location of points at a given altitude $h = R - R_{moon}$, or a given value of dm/dA, at time t requires a (simple) numerical search. In addition, we calculate the apparent radius of the contours of dm/dA as seen from a moving point (the S-S/C). Again, for simplicity, we assume the spacecraft follows the impactor on a vertical trajectory at constant velocity v_{esc}, starting from a specified altitude h_L at $t = 0$.

Below we calculate the relation between dm/dA and the intensity of sunlight reflected by the ejecta as observed by a detector on the shepherding spacecraft given a number of simple assumptions about the instrument characteristics.

Ejecta Curtain Detectability

We start at the "emitter" end, namely the ejecta particles. We assume that ejecta will be seen by reflected sunlight. The solar luminosity is $L_{\odot} = 3.83 \times 10^{26}$ J s^{-1}. The flux at the moon is $L_{\odot}/(4\pi a^2)$, where $a = 1.498 \times 10^{11}$ m. The amount of energy intercepted by a particle of diameter d is then

$$\left(\frac{L}{4\pi a^2}\right)\left(\frac{\pi d^2}{4}\right), \tag{5}$$

and energy reflected to space will be

$$F = \left(\frac{L}{4\pi a^2}\right)\left(\frac{\pi d^2}{4}\right)\frac{\varepsilon}{2\pi}, \tag{6}$$

where ε is the particle's albedo, and we have ignored all issues of anisotropy and scattering, and simply assumed isotropic emission into 2π steradians.

The number of emitters per unit area of the ejecta curtain will be $(1/m_i)(dm/dA)$, where dm/dA is the mass per unit area (which we have calculated from the scaling relations and ballistic dynamics of ejecta), and m_i the typical particle mass.

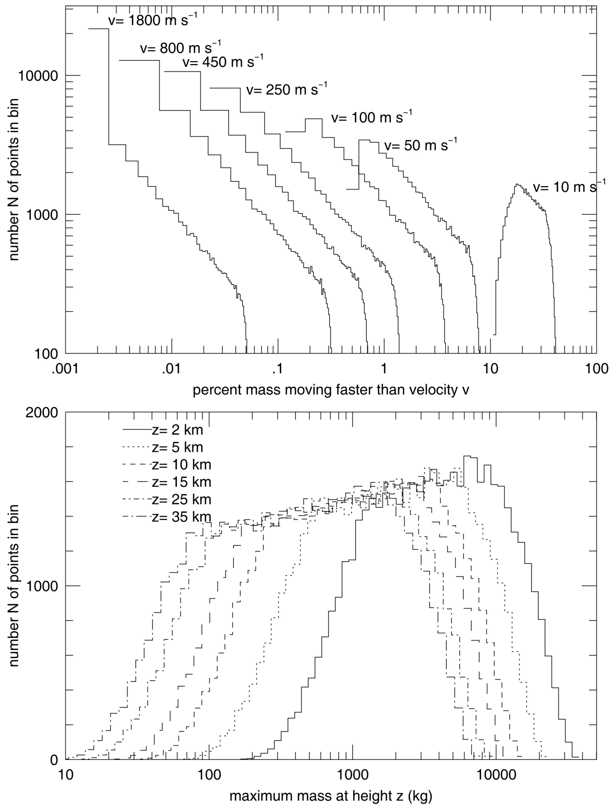

Fig. 11. Top: Monte-Carlo-model results for the distribution of mass versus velocity. The histograms show the number of models that resulted in given percentages of mass moving faster than specified velocities v as labeled on each histogram. Bottom: Monte-Carlo-model results for the distribution of maximum amounts of mass at given heights z after the impact for the same models. Values of model parameters were chosen randomly in the ranges $6.5 < R_{crat} < 11$ m, $2.5 \times 10^5 < M_e < 1 \times 10^6$ kg, $3/7 < \alpha < 3/4$, and $0.2\pi < \theta < 0.3\pi$.

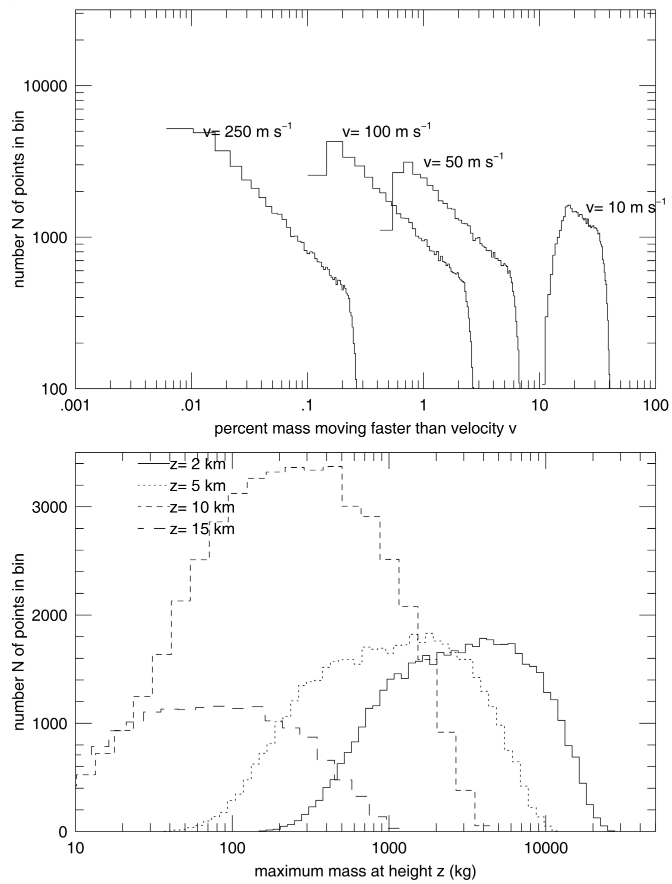

Fig. 12. Top: Monte-Carlo-model results for the distribution of mass versus velocity, now for models with maximum ejecta velocity 300 m s^{-1}. The histograms show the number of models that resulted in given percentages of mass moving faster than specified velocities v as labeled on each histogram. Bottom: Monte-Carlo-model results for the distribution of maximum amounts of mass at given heights z after the impact for the same models. Note that the vertical scale is different from the corresponding panel of Fig. 6. Values of model parameters were chosen randomly in the ranges $6.5 < R_{crat} < 11$ m, $2.5 \times 10^5 < M_e < 1 \times 10^6$ kg, $3/7 < \alpha < 3/4$, and $0.2\pi < \theta < 0.3\pi$.

Again for simplicity, we assume that ejecta are in the form of particles of mass $m_i = \pi\rho_i d_i^3/6$ for particles of diameter d_i. (For the usual power-law distribution of particle diameters, the cross-section of the ejecta will dominated by small particles; the difference in total cross-section will be different by a factor of order unity.) Thus the reflected energy per unit area per steradian will be

$$I = \left(\frac{L}{4\pi a^2}\right)\left(\frac{\pi d^2}{4}\right)\frac{\varepsilon}{2\pi}\left(\frac{6}{\pi\rho_i d^3}\right)\left(\frac{dm}{dA}\right). \tag{7}$$

Putting in numbers, we get

$$I = 1.2\times 10^2\left(\frac{\varepsilon}{0.1}\right)\left(\frac{\rho_i}{2700\ \mathrm{kg\ m^{-3}}}\right)^{-1}\left(\frac{d}{10^2\mu\mathrm{m}}\right)^{-1} \times\left(\frac{dm/dA}{1\ \mathrm{kg\ m^{-2}}}\right)^{-1}\ \mathrm{J\ m^{-2}sr^{-1}s^{-1}}. \tag{8}$$

Note that $(\rho d)^{-1}$ cancels dm/dA, leaving us with the usual units for the intensity I.

Turning to the detector, let the detector area be $\tilde{A}$ with resolution N (i.e., N of pixels on a side). The detector area/pixel is $\tilde{A}/N^2$ and the solid angle subtended by each pixel, as seen from the source, is $\omega = \tilde{A}/N^2D^2$, if the detector is at distance D from the source. Likewise, let the projected area (dimensional area, not solid angle) of a pixel on the source be $\Omega = (D\Theta/N)^2$, where Θ is the field of view in radians.

The easiest quantity to think about in the detector is the number of photons n detected in an integration period Δt. The associated energy is $nh\nu$, where $h\nu$ is the energy of a typical photon. For 5000 Å $h\nu = 4 \times 10^{-19}$ J. Thus, the total energy received by a pixel at the detector equals (the intensity) × (area of pixel) × (solid angle of source seen by the pixel) × (integration period), or $nh\nu = I\Omega\omega\Delta t$.

Rearranging to solve for n, and substituting for Ω and ω, the number of photons per pixel at the detector will be

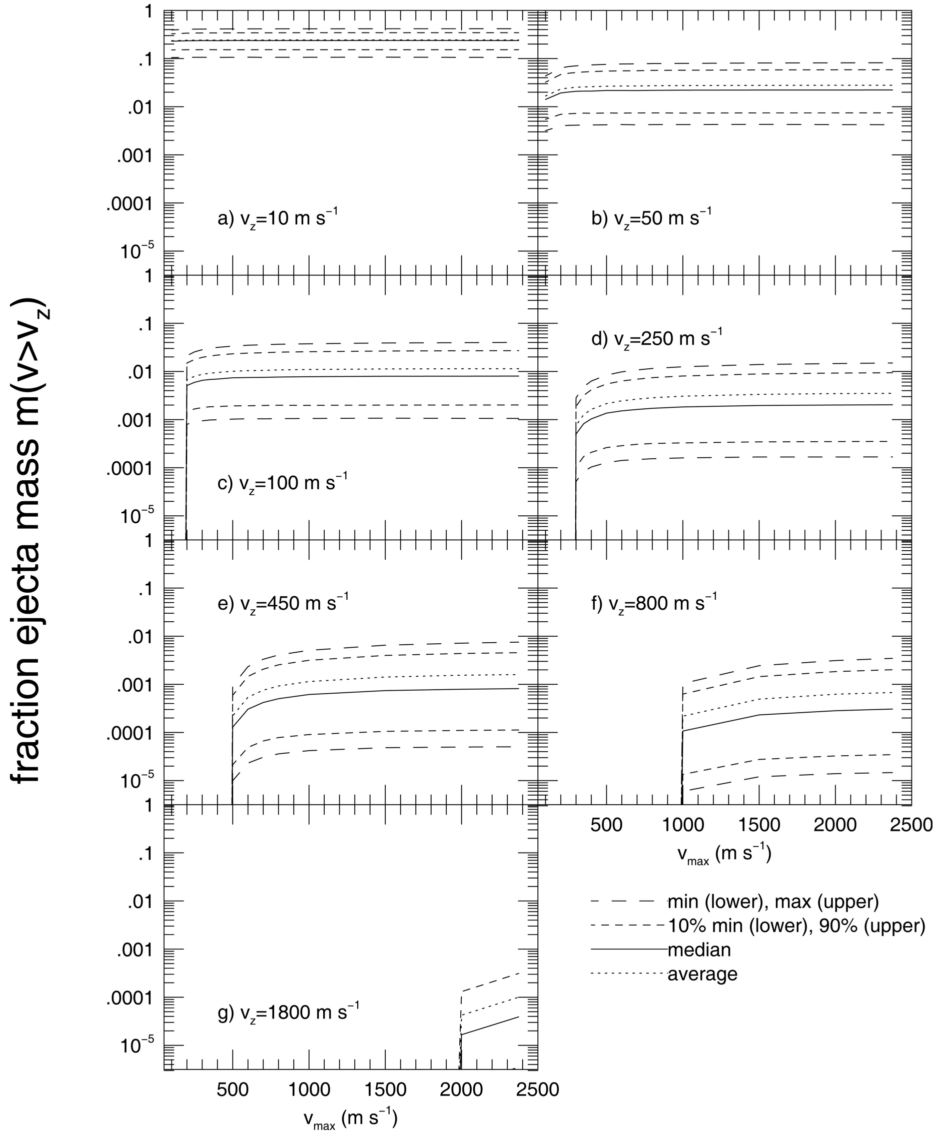

Fig. 13. Monte-Carlo-model results for the fraction of ejecta mass $m(>v_z)$ moving faster than vertical velocity v_z, as a function of maximum ejecta velocity v_{max}. Long-dashed lines show the minimum model (lower line) and maximum model (upper line). Short-dashed lines show $m(>v_z)$ values for the 10% (lower line) and 90% models. The dashed line shows that average value and the dotted line the median value of $m(>v_z)$ for the given value of v_z: a) $v_z = 10$ m s^{-1}, b) $v_z = 50$ m s^{-1}, c) $v_z = 100$ m s^{-1}, d) $v_z = 250$ m s^{-1}, e) $v_z = 450$ m s^{-1}, f) $v_z = 800$ m s^{-1}, and g) $v_z = 1800$ m s^{-1}. Values of model parameters were chosen randomly in the ranges $6.5 < R_{crat} < 11$m, $2.5 \times 10^5 < M_e < 1 \times 10^6$ kg, $3/7 < \alpha < 3/4$, and $0.2\pi < \theta < 0.3\pi$.

$$n = \frac{I\Delta t}{h\nu}\Omega\omega = \frac{I\Delta t}{h\nu}\left(\frac{D^2\Theta^2}{N^2}\right)\left(\frac{\tilde{A}}{D^2N^2}\right) = \frac{I\Delta t}{h\nu}\left(\frac{\tilde{A}\Theta^2}{N^4}\right) \tag{9}$$

Substituting for I from Equation 8 we have

$$n = 7.5\times10^3\left(\frac{\varepsilon}{0.1}\right)\left(\frac{\rho_i}{2700\ \mathrm{kg\ m^{-3}}}\right)^{-1}\left(\frac{d}{10^2\mu\mathrm{m}}\right)^{-1}\left(\frac{dm/dA}{1\ \mathrm{kg\ m^{-2}}}\right)^{-1}$$

$$\times\left(\frac{\Delta t}{1\mathrm{s}}\right)\left(\frac{N}{10^3\ \mathrm{pixels}}\right)^{-4}\left(\frac{\tilde{A}}{2.5\times10^{-3}\mathrm{m}^2}\right)\left(\frac{\Theta}{10^{-1}\ \mathrm{rad}}\right)^2. \tag{10}$$

We can rewrite this to solve for the required dm/dA for given values of the parameters:

$$\frac{dm}{dA} = 1.3\times10^{-4}\left(\frac{n}{1\ \mathrm{photon}}\right)\left(\frac{\Delta t}{1\mathrm{s}}\right)^{-1}\left(\frac{\varepsilon}{0.1}\right)^{-1}\left(\frac{\rho_i}{2700\ \mathrm{kg\ m^{-3}}}\right)\left(\frac{d}{10^2\mu\mathrm{m}}\right)$$

$$\times\left(\frac{N}{10^3\ \mathrm{pixels}}\right)^4\left(\frac{\tilde{A}}{2.5\times10^{-3}\mathrm{m}^2}\right)^{-1}\left(\frac{\Theta}{10^{-1}\ \mathrm{rad}}\right)^{-2}\ \mathrm{kg\ m^{-2}}. \tag{11}$$

That is, given values of n, Δt, etc., Equation 11 gives the minimum value of dm/dA needed for a detection in that pixel.

To examine how the ejecta curtain might evolve and how detectable it might be, We have calculated two sets of quantities: a) the height of levels of dm/dA as a function of time t after the impact at $t = 0$, and the angular radius θ_L of contours

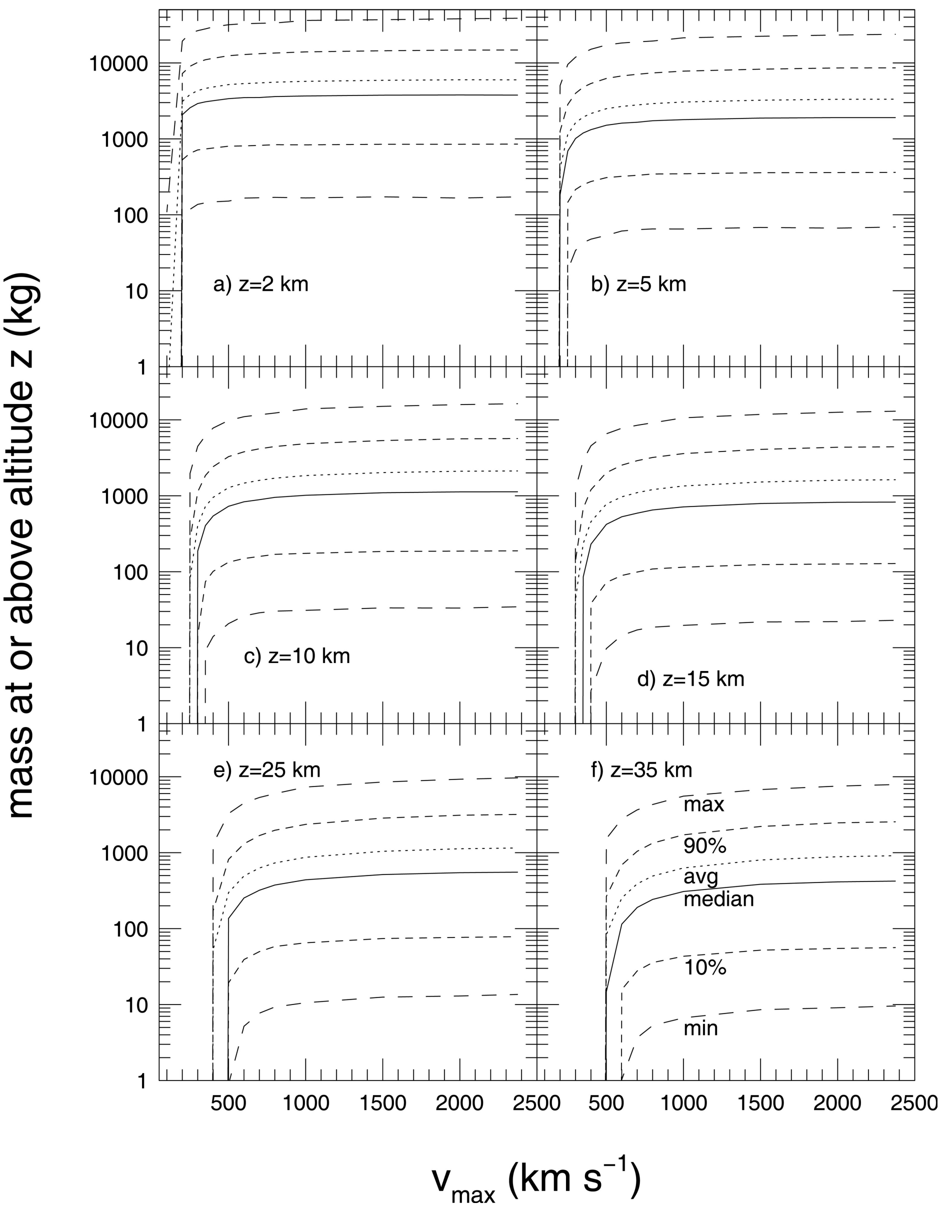

Fig. 14. Monte-Carlo-model results for the ejecta mass $m(z)$ that reaches height z, as a function of maximum ejecta velocity v_{max}. Long-dashed lines show the minimum model (lower line) and maximum model (upper line). Short-dashed lines show $m(>v_z)$ values for the 10% (lower line) and 90% models. The dashed line shows that average value and the dotted line the median value of $m(z)$ for the given value of v_z: a) $z = 2$ km, b) $z = 5$ km, c) $z = 10$ km, d) $z = 15$ km, e) $z = 25$ km, f) $z = 35$ km. Values of model parameters were chosen randomly in the ranges $6.5 < R_{crat} < 11$ m, $2.5 \times 10^5 < M_e < 1 \times 10^6$ kg, $3/7 < \alpha < 3/4$, and $0.2\pi < \theta < 0.3\pi$.

of dm/dA as seen in the field of view of an observer (the shepherding spacecraft), as a function of time, assuming that the S-S/C is coming in at a specified velocity v_L to impact at a specified time t_L. In this case, we have chosen $t_L = 240$ s and $v_L = v_{esc} \approx 2.4$ km s^{-1}.

Figure 15 shows plots of the height (top) and angular radius (bottom) of the loci of ejecta curtain surface densities dm/dA as functions of time. Top panel: height z of specified ejecta surface densities as a function of time. Parameters are: total ejecta mass $M_e = 10^6$ kg, ejecta power law index $\alpha = 3/5$. Minimum and maximum ejecta velocities are $v_{min} = 4.03$ m s^{-1} (corresponding to a crater 20 m in diameter) and $v_{max} = v_{esc} = 2.38 \times 10^3$ ms^{-1}. For 100 µm particles with albedo $\varepsilon = 0.1$, a column density of $dm/dA = 10^{-6}$ kg m^{-2} corresponds to ~1 photon per pixel per second for a detector of aperture area $\tilde{A} = 0.25$ m^2, $N = 1000$ pixel resolution and angular aperture $\Theta = 0.1$ radian. Bottom panel: angular radius of contours of ejecta curtain surface density dm/dA as a function of time as seen by an observer on a vertical trajectory starting at $h = 576$ km at EDUS impact ($t = 0$) and downward velocity $v_{esc} = 2.4$ km s^{-1}. The dotted line shows the angular radius of the inner edge on the ground of the ejecta curtain as a function of time.

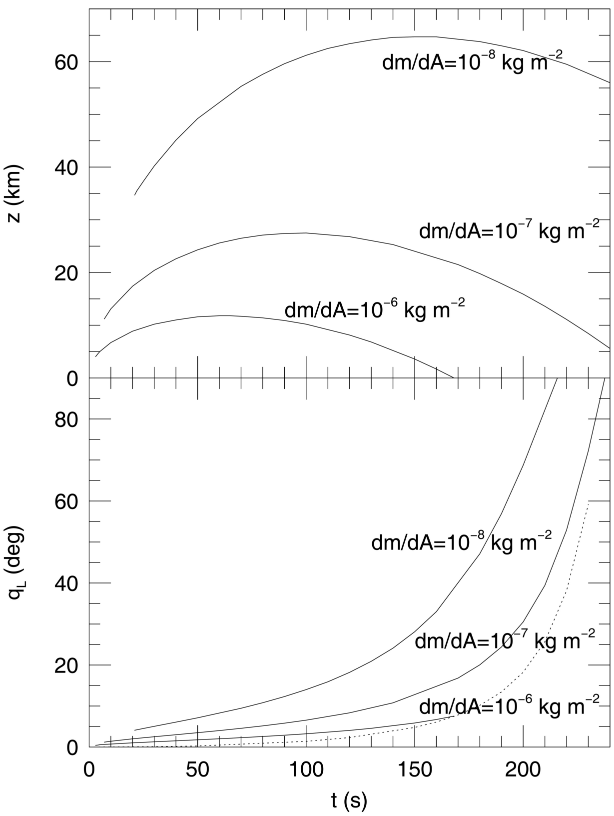

Fig. 15. Top: height z of specified ejecta surface densities as a function of time. Parameters are: total ejecta mass $M_e = 10^6$ kg, ejecta power law index $\alpha = 3/5$. Minimum and maximum ejecta velocities are $v_{min} = 4.03$ m s^{-1} (corresponding to a crater 20 m in diameter) and $v_{max} = v_{esc} = 2.38 \times 10^3$ m s^{-1}. Bottom: angular radius of contours of ejecta curtain surface density dm/dA as a function of time, as seen by the S-S/C on a vertical trajectory starting at h = 576 km at EDUS impact ($t = 0$) and downward velocity $v_{esc} = 2.4$ km s^{-1}, so that S-S/C strikes the surface at t = 240 s. The solid lines correspond to ejecta surface densities as labeled, while the dashed line shows the angular extent of the inner edge of the ejecta curtain that intersects the surface.

CONCLUSIONS

We have modeled various phases of the upcoming LCROSS impact mission, using several different tools, including the RAGE and ZEUS-MP finite difference hydrodynamics codes, a smooth-particle hydrodynamics (SPH) code, and semi-analytic calculations based on empirical crater scaling models. RAGE was used to model the initial short time scale hot plume immediately after impact; the calculation produced a quasi-spherical hot plume expanding at speeds up to 7 km s^{-1} and temperatures up to ~1200 K. Such an impact flash might be detectable by the LCROSS instruments in the first 0.1 s after impact, in particular the Total Luminescent Photometer (TLP). The flash will have a visible component that the mission will attempt to measure with the TLP, which can measure down to ~0.1 nW with a sample rate of 1000 Hz. Assuming a luminosity efficiency factor η for the impact of 10^{-4} to 10^{-5} (Ernst and Schultz 2005, 2007), or about 1−10 nW at the TLP detector, the visible flash is expected to last about 0.1 s. The mission will also measure the entire flash color (integrating across the entire duration of the flash) with the UV/Vis spectrometer. The near-infrared (NIR) portion of the flash is the thermal part (the radiation from the ~1200 K temperature of the initial plume). We expect it to peak between 2–3 microns. The mission will measure the flash with the NIR spectrometers (in flash mode) and the NIR cameras (which go out to about 2.5 microns). The spectrometers and NIR cameras are very sensitive. The MIR cameras only go down to 7 micron and so not much may be seen at long wavelengths. For comparison, the SMART-1 flash was easily detected by the Canada-France-Hawaii Telescope (Veillet 2006, 2007; Veillet et al. 2006; Veillet and Foing 2007). Note, however, that the only component of the SMART-1 impact flash visible from Earth was due to the burning of residual hydrazine, as indicated by spectrometry on the flash. Our models do not take hydrazine into account, and there is some uncertainty as to how much will be left, and how much that will affect the flash and H and O estimates. We regard hydrazine contamination as the chief uncertainty on the volatile content estimate and on the impact flash/plume IR visibility.

Crater scaling relationships and the SPH calculation suggest that a crater 11–20 m in diameter and several meters deep will be produced by the impact. An impact ejecta curtain with material velocity up to ~1 km s^{-1} was also produced by the same calculations. For reasons that are unclear, ZEUS-MP produced a much larger crater (up to nearly 80 m in diameter) and correspondingly greater mass of ejecta. The velocity distribution of the ejecta (mass m ($>v$) moving at velocity v or larger) was similar to that predicted by the SPH calculation. Aside from the ZEUS-MP crater dimensions, the results of our calculations are also similar to those done by Shuvalov and Trubetskaya (2008). SPH calculations predict that m ($z >$ 2 km) ~2×10^4 kg of ejecta will reach heights of 2 km or higher.

Monte Carlo calculations based on crater scaling relations are more conservative in their predictions, with a median estimate m ($z >$ 2 km) ~$2 - 4 \times 10^3$ kg at 2 km, depending on the maximum velocity of the ejecta.

Acknowledgments–We thank Professor Jennifer Anderson and an anonymous reviewer for comments that have improved the manuscript.

Editorial Handling—Dr. Carlé Pieters

REFERENCES

Benz W. and Asphaug E. 1994. Impact simulations with fracture. I. Method and tests. *Icarus* 107:98–116.

Bond V. R. and Allman M. C. 1996. *Modern astrodynamics:*

Fundamentals and perturbation methods. Princeton, N. J.: Princeton University Press. 250 p.
Ernst C. M. and Schultz P. H. 2005. Investigations of the luminous energy and luminous efficiency of experimental impacts into particulate targets (abstract #1475). 36th Lunar and Planetary Science Conference. CD-ROM.
Ernst C. M. and Schultz P. H. 2007. Evolution of the Deep Impact flash: Implications for the nucleus surface based on laboratory experiments. *Icarus* 190:334–344.
Gittings M., Weaver R., Clover M., Betlach T., Byrne N., Coker R., Dendy E., Hueckstaedt R., New K., Oakes W. R., Ranta D., and Stefan R. 2008. The RAGE radiation-hydrodynamic code. *Computational Science and Discovery* 1:015005.
Grady D. E. and Kipp M. E. 1980. Continuum modelling of explosive fracture in oil shale. *International Journal of Rock Mechanics and Mining Science & Geomechanics Abstracts* 17:147–157.
Harten A., Lax P., and Van Leer B. 1983. On upstream differencing and Godunov-type schemes for hyperbolic conservation laws. *SIAM Review* 25:35–61.
Heiken G. H., Vaniman D. T., and French B. T. 1991. *The Lunar source book: A user's guide to the moon.* Cambridge, UK: Cambridge University Press. 736 p.
Herrmann W. 1969. Constitutive equation for the dynamic compaction of ductile porous materials. *Journal of Applied Physics* 40:2490–2499.
Holsapple K. A. 1987. The scaling of impact phenomena. *International Journal of Impact Engineering* 5:343–355.
Holsapple K. A. 1993. The scaling of impact processes in planetary sciences. *Annual Review of Earth and Planetary Science* 21:333–373.
Holsapple K. A. 2007. Crater sizes from impacts or explosions (web site): http://keith.aa.washington.edu/craterdata/scaling/index.htm. Accessed 30 April 2009.
Holsapple K. A. and Schmidt R. M. 1982. On the scaling of crater dimensions 2. Impact processes. *Journal of Geophysical Research* 87:1849–1870.
Housen K. R., Schmidt R. M., and Holsapple K. 1983. Crater ejecta scaling laws: Fundamental forms based on dimensional analysis. *Journal of Geophysical Research* 88:2485–2499.
Jutzi M., Benz W., and Michel P. 2008. Implementing micro-scale porosity in a 3D SPH hydrocode. *Icarus* 198:242–255.
Kamm J. R. and Rider W. J. 1998. 2-D convergence analysis of the RAGE hydrocode. Los Alamos National Laboratory Technical Report LA-UR-98-3872.
Korycansky D. G., Zahnle K. J., and Mac Low M.-M. 2002. High resolution simulations of the impacts of asteroids into the venusian atmosphere 2: 3D Models. *Icarus* 157:1–23.
Korycansky D. G. and Zahnle K. J. 2003. High resolution simulations of the impacts of asteroids into the Venusian atmosphere III: Further 3D Models. *Icarus* 161:244–261.
Korycansky D. G., Harrington J., Deming D., and Kulick M. E. 2006. Shoemaker-Levy 9 impact modeling: I. High-resolution 3D bolides. *The Astrophysical Journal* 646:642–652.
Libersky L. D. and Petschek A. G. 1991. Smooth Particle hydrodynamics with strength of materials. In *Proceeding Next Free-Lagrange Method*, edited by Trease Fritts. Crowley Lecture Notes in Physics, vol. 395. Berlin: Springer-Verlag. pp. 248–257.
Melosh H. J. 1989. *Impact cratering*. New York: Oxford University Press. 245 p.
Michel P., Benz W., Tanga P., and Richardson D. C. 2001. Collisions and gravitational reaccumulation: Forming asteroid families and satellites. *Science* 294:1696–1700.
Norman M. 2000. Introducing ZEUS-MP: A 3D, parallel, multiphysics code for astrophysical fluid dynamics. In *Astrophysical plasmas: Codes, models, and observations*, edited by Arthur J., Brickhouse N., and Franco J. Mexico D. F.: Instituto de Astronomía, Universidad Nacional Autónoma de México.
O'Keefe J. D. and Ahrens T. J. 1993. Planetary cratering mechanics. *Journal of Geophysical Research* 98:17,011–17,028.
Schmidt R. M. and Holsapple K. A. 1983. Theory and experiments on centrifuge cratering. *Journal of Geophysical Research* 85: 235–252.
Schultz P. H. and Gault D. E. 1985. Clustered impacts: Experiments and implications. *Journal of Geophysical Research* 90B5:3701–3732.
Shuvalov V. V. and Trubetskaya I. A. 2008. Numerical simulation of the LCROSS impact experiment. *Solar System Research* 42:1–7.
Veillet C. 2006. SMART-1 impact website, http://www.cfht.hawaii.edu/News/Smart1/.
Veillet C. 2007. The impact plume of the SMART-1 impact. AAS Meeting 210, abstract 42.01. *Bulletin of the American Astronomical Society* 38:156.
Veillet C., Albert L., Foing B., and Ehrenfreund P. 2006 CFHT observation of SMART-1 impact. American Astronomical Society, DPS Meeting 38, abstract 57.17. *Bulletin of the American Astronomical Society* 38:1303.
Veillet C. and Foing B. 2007. SMART-1 impact observation at the Canada-France-Hawaii Telescope (abstract #1520). 38th Lunar and Planetary Science Conference. CD-ROM.